Switching from brittle to ductile isotactic polypropylene-g-maleic anhydride by crosslinking with capped-end polyether diamine

Adrien Létoffé, Santiago García-Rodríguez, Sandrine Hoppe, Nadia Canilho, Olivier Godard, Andreea Pasc, Isabelle Royaud, Marc Ponçot

▶ **To cite this version:**

Adrien Létoffé, Santiago García-Rodríguez, Sandrine Hoppe, Nadia Canilho, Olivier Godard, et al.. Switching from brittle to ductile isotactic polypropylene-g-maleic anhydride by crosslinking with capped-end polyether diamine. Polymer, 2019, 164, pp.67-78. 10.1016/j.polymer.2019.01.015 . hal-01977587

HAL Id: hal-01977587
https://hal.science/hal-01977587

Submitted on 21 Oct 2021

HAL is a multi-disciplinary open access archive for the deposit and dissemination of scientific research documents, whether they are published or not. The documents may come from teaching and research institutions in France or abroad, or from public or private research centers.

L'archive ouverte pluridisciplinaire **HAL**, est destinée au dépôt et à la diffusion de documents scientifiques de niveau recherche, publiés ou non, émanant des établissements d'enseignement et de recherche français ou étrangers, des laboratoires publics ou privés.

Distributed under a Creative Commons Attribution - NonCommercial 4.0 International License

Version of Record: https://www.sciencedirect.com/science/article/pii/S0032386119300242
Manuscript_fe4ae81cc730e54a6b51d0a4165c8ebd

Switching from brittle to ductile isotactic polypropylene-*g*-maleic anhydride by crosslinking with capped-end polyether diamine

Adrien Létoffé [a,b], Santiago M. García-Rodríguez [a,b], Sandrine Hoppe[c], Nadia Canilho[d], Olivier Godard [a], Andreea Pasc [d], Isabelle Royaud[a], Marc Ponçot[*a,b]

[a]Université de Lorraine, CNRS, IJL, F-54000 Nancy, France
[b]Université de Lorraine, CNRS, LabEX "DAMAS", F-57000 Metz, France
[c]Université de Lorraine, CNRS, LRGP, F-54000 Nancy, France
[d]L2CM UMR CNRS 7053, Université de Lorraine, F-54506, Vandœuvre-lès-Nancy, France

ABSTRACT:

Ductile functionalized polypropylene is of great interest in multi-layer composites development. A capped-end triblock polyether diamine (H_2N-PO_2-TMO_9-PO_3-NH_2) was used as a linker of two different maleated isotactic polypropylenes (iPP-*g*-MAH, at 1 and 3 wt%) by twin-screw reactive extrusion. The molecular architecture, the semi-crystalline microstructure and the mechanical properties of the resulting polymers were analysed as a function of the molar ratio of NH_2:MAH (0:1, 0.33:1, 0.5:1, 0.66:1, 1:1, 1.5:1, 2:1). At the molecular scale, the chemically modified polymers were characterized by FTIR and by the determination of gel content following the ASTM D2765-84 standard method. Differential Scanning Calorimetry, Wide Angle X-rays Scattering and Self Successive Auto-nucleation techniques showed the impact of the crosslinking: a decrease of the melting temperature as compared with the unmodified iPP-*g*-MAH polymer, as well as a decrease of the crystallinity ratio for the iPP-*g*-MAH at 3 wt% of MAH. Interestingly, Dynamic Mechanical Analysis and video-controlled uniaxial tensile tests showed that the polymers obtained in stoichiometric NH_2:MAH molar ratio exhibit the best mechanical properties enlightened by a switch from brittle to ductile mechanical behaviour with few differences between the two iPP-*g*-MAH.

KEYWORDS: *isotactic polypropylene grafted maleic anhydride, polyether diamine, crosslinking, microstructure, molecular architecture, mechanical properties.*

1. Introduction

Environmental impact became nowadays of paramount importance to material production, in both fundamental research and industry. For example, transport accounts for 25% of global CO_2 emission, which has a direct influence on climate change. Reducing fuel consumption and thus CO_2 emission in transport could be gathered by engineering efficient combustion engines and/or by lighter transporters structures. Composite materials, such as multi-layered steel/polymer composites, appear as good candidates for lighter structures. Among polymers, isotactic polypropylene-maleic anhydride (iPP-*g*-MAH) combines properties of iPP, such as low cost, low density and easy processing ability with the ones of anhydride moiety that ensures a good compatibility with the metal surfaces.

The grafting of MAH onto iPP, firstly reported by Minoura *et al.*, can be carried out in the melting state [1-5], but also in solid state or in solution [6-10]. The grafting undergoes undesirable side reactions, like chain scission, that modifies the average molecular weight of the material [1-11]. For instance, Shi *et al.* reported a reduction of about 76% of the weight-average $\overline{M_w}$ of an iPP-*g*-MAH made by reactive extrusion (with 0.78 wt% of MAH) [11]. This is the major drawback of this reaction, since it affects the final mechanical properties of the polymer characterized by a brittle

© 2019 published by Elsevier. This manuscript is made available under the CC BY NC user license
https://creativecommons.org/licenses/by-nc/4.0/

fracture. As a result, it becomes inefficient in shock absorption due to the absence of plasticity and in particular volume damage. The MAH grafts also affect the microstructure of the material. Seo *et al*. and Harper *et al*. reported a good miscibility between the graft and the unmodified polymer chains, as well as a decrease of the melting temperature range with the MAH weight fraction inside the material [12, 13].

To improve the mechanical properties, we proposed in this work to increase the crosslinking within the polymer, by using a polyether diamine. As a matter of fact, different crosslinking methods have been developed in the last ten years. For example, Kubo *et al*. used hydrogen donating hydrocarbons stabilizer to prevent β-scission degradation during the irradiation with an electron beam [14]. Other authors used polyfonctional monomers as crosslinking agent [15], or dicumyl peroxide molecules as a chemical initiator, to trigger a crosslinking reaction with a peroxide/sulphur/accelerator system [16-19]. Those different crosslinking reactions show an important impact on the microstructure [14-19]. A decrease of the crystallinity ratio and the crystal sizes could be observed. This evolution was correlated with an increase of the viscosity due to the loss of the polymer chain mobility.

The crosslinking reaction proposed in this work (Scheme 1) is based on the reaction between maleic anhydride (MAH) and amino groups (NH_2) [20, 21]. This kind of reaction, implying NH_2 in excess, has already been used and it lead to a chain extension of iPP-*g*-MAH [22-24], and thus to new reactive sites (e.g. amino groups) in the polymeric material [25, 26]. The reaction and those new functionalities could be used as a coupling agent for copolymers like PP/PE [27] or PP/PA6 [28]. It could also allow an enhanced dispersion of nano-fillers inside polymers [29, 30]. The wide variety of the reaction applications make it particularly suitable for composites production, and provide new properties to iPP. An interesting result, obtained by Lu *et al.* [26], was the evolution of the mechanical properties of an iPP-*g*-MAH functionalized with a large excess of diamine. Their material, an iPP-*g*-MAH with 0.55wt% of MAH grafts, was functionalized with small diamine molecules at a NH_2:MAH molar ratio of 3:1. It was observed that a significant raise of strain and stress at break occurred. However, in the particular case of diamine excess, the reaction only induced a polymer chain extension without creating a three-dimensional macromolecular network. In this work, the evolution of the microstructure and the mechanical properties of iPP-*g*-MAH with respectively 1 wt% and 3 wt% of MAH, functionalized with a polyether diamine for different NH_2:MAH molar ratios were investigated. The objective was to determine the optimal formulation (weight fraction of MAH and NH_2:MAH molar ratio) having the best mechanical properties. Molar ratios below and above equimolarity (from 0.33:1 to 2:1) were tested. The impact of the reaction on the molecular architecture was characterized by FTIR and the gel content standard method. The modifications of the semi-crystalline microstructure were investigated by the self-successive auto-nucleation technique (SSA) and X-ray scattering. The close relationship with the true mechanical behaviour was highlighted by VidéoTraction™ system, after taking into account or not the volume strain.

2. Materials preparation

2.1 Materials

Two different maleated isotactic polypropylenes were studied in this work. The first one is an isotactic polypropylene grafted with 1 wt% of maleic anhydride (noted CA 100). The polymer is supplied by Arkema under the commercial name Orevac®

CA100. According to the technical specification sheet provided by Arkema [29], the yield strength is 22 MPa, and the engineering elongation at break is 12%. Its average molecular weight is estimated at $\overline{M_n}$= 25 000 g.mol^{-1} [30, 31]. Prior to our experiments, conventional experiments have been done to determine the nature of the crystalline phase and the crystallinity ratio of CA 100. The main melting temperature, after the thermomechanical history erasing, was measured at 162°C by differential scanning calorimetry (DSC) at 10°C/min. This temperature is consistent with the melting of α-phase crystals, which were also revealed by wide angles X-rays scattering analysis (WAXS). The crystallinity ratio was determined by DSC and WAXS measurements and was of 55 ± 3% and 62 ± 3% respectively.

The second polymer used in this work is also an isotactic polypropylene grafted by maleic anhydride units, but in a larger amount of 3 wt%. It was supplied by Eastman™ under the commercial name Eastman™ G-3015 (noted G 3015). The technical specification sheet informed us about the average molecular weights that are $\overline{M_n}$= 24 000 g·mol^{-1} and $\overline{M_w}$= 47 000 g·mol^{-1} [32-34]. No more information about the mechanical properties is given. As for the CA 100, the melting temperature of 162°C revealed by DSC and the WAXS measurements confirmed the presence of crystals in the α-phase. The crystallinity ratio of G 3015 was estimated to be around 55 ± 3% by DSC and 61 ± 3% by WAXS. The MAH weight fractions of the two starting polymers were precisely determined by elemental analysis to be of 1.16 wt% for the CA 100 and of 2.9 wt% for the G 3015, respectively (see Table S1 in SI).

The crosslinking agent used in this work is a capped-end triblock polyether diamine (H_2N-PO_2-TMO_9-PO_3-NH_2), commercialized as Jeffamine® THF 100 by Huntsman [7] and used as received. Jeffamine® THF 100 (noted THF100) is a capped-end diamine copolymer of poly(tetramethylene ether glycol) (PTMEG) and polypropylene glycol (PPG), with a molecular weight of 1000 g·mol^{-1}. THF100 is liquid at room temperature and atmospheric pressure. The Jeffamine® was mostly chosen because the reactivity of aliphatic primary amines on maleic anhydride group is higher compared to aromatic amines [27]. Moreover, the high molecular weight of polyether diamine with a melting point at 9°C and a flash point at 238°C prevents any evaporation or degradation of the crosslinker during the reactive extrusion process.

2.2 Materials Preparation

The reaction between the MAH and the diamine, shown on Scheme 1, is divided in two steps. First, one amino group reacts with the anhydride, which leads to an amide and a carboxylic acid. This reaction takes place at room temperature. The second step, the cyclization one, is much slower and undergoes at the melting temperatures of the iPP-*g*-MAH [25-27].

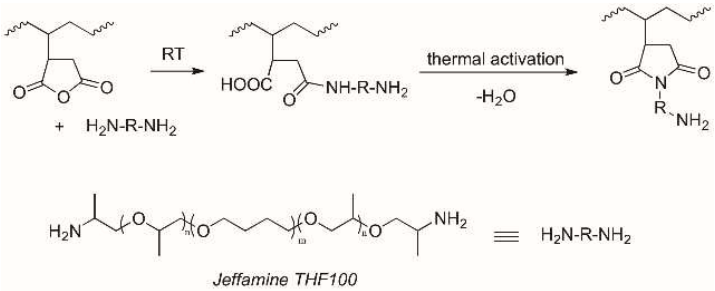

Scheme 1. Reaction pathway affording to the crosslinking between THF-100 and iPP-*g*-MAH through either amide or imide bonds.

The chemical reaction process was run either at the CINI Company or at the LRGP laboratory (CNRS - University of Lorraine, Nancy, France), using a 10 mm barrel extruder (Twinscrew Benchtop Compounding Line developed by Rondol Technology Ltd). Its L:D ratio is 40:1. Seven different intermediate temperature areas (Table 1) composed the extruder barrel between the pellet feed hopper and the rod shaped outlet die. The rotation speed was fixed at a specific value of 20 rpm in order to maintain a reaction time between 5 and 7 min (reaction time inside the extruder barrel after adding the THF 100), depending on the NH_2:MAH molar ratio and the material viscosity.

Table 1. Temperature profile of the extruder barrel

Extruder area	Input	Temperature Areas							Die plat
		1	2	3	4	5	6	7	
Temperature (°C)	150	170	190	190	190	190	180	170	170

iPP-*g*-MAH was introduced with a mass flow of 0.6 $g \cdot min^{-1}$ for the CA 100 and 1 $g \cdot min^{-1}$ for the G 3015. The diamine was added in the area 3 of the extruder barrel (at 190°C), and the mass flow rate was adapted to rich the targeted molar ratios NH_2:MAH (ranging from 0:1 to 2:1). The crosslinked iPP-*g*-MAH materials were shaped into 3 mm plates by injection moulding using a Micro 12cc Injection Moulding Machine commercialized by DSM Xplore. The material pellets were molten at 200°C and injected at 100°C under 10 bars. 2D WAXS patterns analysis confirmed the isotropic distribution of the macromolecular chains in the plane of the injected plates. Surface irregularities and microstructural heterogeneities (skin-core structure gradient) were removed by polishing the samples.

3. Experimental set up

3.1. Gel Content measurements

The gel content of the two iPP-*g*-MAH and the functionalized materials were determined following the ASTM D2765-84 standard method. The test was carried out with boiling xylene as an extraction solvent inside a copper pouch. The measurements were performed in triplicate.

3.2. Fourier Transform Infrared (FTIR) spectroscopy and band assignments

FTIR analyses were performed at room temperature using an IRAffinity-1S spectrophotometer commercialized by SHIMADZU. Spectra were recorded in transmission mode in the wavenumbers range of 400 to 4000 cm^{-1} using a 4 cm^{-1} resolution and accumulating 64 scans. Before analysis, the samples, taken from the injected plates, were compressed to obtain films, with a thickness of 50 to 200 µm. The spectra were treated with the Fityk software. To compare the spectrum of each material, a reference band at 998 cm^{-1} (methyl groups rocking) was used to normalize the overall spectral intensity. This vibrational band was chosen since it is not a vibrational band that could change with the reaction such as those associated with imide, amide, MAH or amine groups.

3.3. Wide angles X-rays Scattering (WAXS)

WAXS analyses were performed with a tension and an intensity of 30 kV and 40 mA, respectively. The wavelength used was the copper radiation $K_{\alpha 1}$ (λ= 0.154 nm). A parabolic multilayer mirror (Osmic) and a cylindrical capillary selected the wavelength and shaped the incident beam. The sample used were 1cm x 1 cm square cut in the

middle of the injected plates, and polished from both sides to obtain a 1 mm thickness. Using a rotating sample holder, the analyses represent the average crystal diffraction in the plane of the sample free of any crystalline texture. The 1D diffractograms were deconvoluted using the Hermans and Weidinger method [36]. The contributions of amorphous and crystalline phases were fitted with a series of Gaussian and Lorentzian functions [37, 38]. The crystallinity ratio was calculated as the ratio of the crystalline peaks areas over the total area corresponding to the sum of the areas of the crystalline peaks and the amorphous halo. The 2D analyses were performed with a photosensitive plane film at a distance of 75 mm from the sample that were scanned using a FUJIFILM scanner BASF 5000.

3.4. Differential Scanning Calorimetry analysis (DSC)

The DSC experiments were performed using a Q200 TA Instruments apparatus. The samples, weighing around 10 mg, were taken from the WAXS samples and were encapsulated in aluminium pans and analyzed under an inert flux of nitrogen. To characterize the sample microstructures, the thermal cycle performed at 10°C·min^{-1} consisted in a first heating ramp from 30°C to 200°C at 10°C·min^{-1} to characterize the initial microstructure of the sample, a controlled cooling ramp to 30°C and a second heating ramp to 200°C to study the standard thermal behaviour. The crystallinity ratios of the materials were estimated as follows:

$$X_c = \frac{\Delta H_m}{\Delta H_m^0} \qquad (1)$$

where ΔH_m is the melting enthalpy, and ΔH_m^0=165 J·g^{-1} is the enthalpy of a 100% crystalline isotactic polypropylene [39]. The main crystalline lamellar thickness population (L_c) of the polymer was derived from the Gibbs-Thomson equation:

$$T_m = T_m^0\left(1 - \frac{2\,\sigma_e}{\rho_c \Delta H_m^o L_c}\right) \qquad (2)$$

where T_m is the melting peak temperature measured at the maximum of the endotherms, T_m^0 is the melting temperature of a 100% crystalline isotactic polypropylene, σ_e is the surface free energy of iPP crystalline lamellae and ρ_c the crystalline phase density. T_m^0 is given by the literature at 460 K, σ_e at 0.0496 J.m^{-2}, and ρ_c at 0.9361 g.cm^{-3} [39, 40].

3.5. Successive Self-Nucleation and Annealing (SSA)

SSA experiments were performed to characterize the thickness distribution of the crystallites [41, 42]. This thermal fractionation technique is used to study the semi crystalline polymers with linearity defects in their macromolecular chains (co-monomers, stereo-defects, chains branching, crosslinking…) [43]. For instance, Ogier *et al.* [44] previously used this method to characterize the important decrease of the main lamellar thicknesses of PE orthorhombic crystals as a function of the crosslinking degree of an ethylene-co-vinyl acetate polymer. This method could also be used to study the length distribution inside a polymer like polypropylene [45, 46]. The SSA protocol is initiated at a specific temperature, called ideal self-nucleation temperature T_S, which was previously determined by a self-nucleation (SN) analysis. In case of comparison of the thermal fractionation behaviours of chemically modified semi-crystalline polymers, the material used to identify T_s is the one that presents the highest melting temperature, which is neat CA 100 for the CA 100 materials, and neat G3015 for the G 3015 materials [46]. The SN protocol and is application is presented in the supporting information.

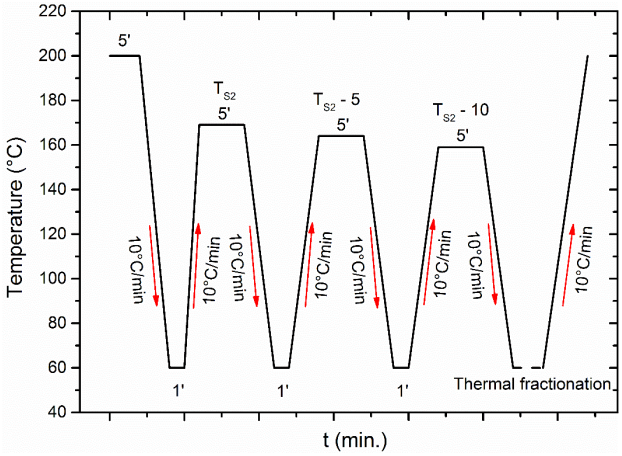

Fig.1. Temperature profile of the SSA crystal fractionation method.

Once the T_s was determined, the SSA protocol illustrated in Fig.1 can be carried out as follows:

- The thermomechanical history of the elaborated samples is firstly erased by a rapid heating ramp above the melting temperature at 200 °C for 3 min. then followed by a controlled cooling ramp to 60 °C at 10 °C/min to ensure for all materials the same thermal history.
- Heating up to T_{s2}, and holding this temperature for 5 min.
- Cooling down to 60 °C at 10 °C.min^{-1}.
- Heating up to a new temperature T_s, 5 °C lower than the previous one and remaining 5 min.
- Repeating the two last steps until the achievement of seven different T_s temperatures.
- Carrying out a final heating, up to 200 °C to melt all the fractionated crystals.

3.6. Dynamic mechanical analysis (DMA):

The dynamic mechanical properties of the materials were determined using a DMA 242C commercialized by Netzsch. Rectangular bar shaped samples of dimension 20 x 4 x 3 mm^3 were machined out in the injected plates. Measurements of the complex modulus were performed in three points bending mode at three different frequencies (1, 5 and 10 Hz) in the temperatures range from -150 °C to 130 °C and at a constant heating rate of 2 °C.min^{-1}. The complex modulus is composed of the storage modulus E' (real part) and the loss modulus E'' (imaginary part). E' represents the storage modulus material and is proportional to the energy stored during a loading cycle. It corresponds to the elastic Young modulus. E'' represents the loss modulus from the viscous part of the polymer. The loss factor tan δ is then defined as the ratio of the loss modulus to storage modulus. Results of i) storage modulus (E'), and ii) loss factor ($\tan\delta = E''/E'$) are represented as a function of temperature for three frequencies.

3.7. Mechanical testing:

The true mechanical behaviours of the different materials were determined using the VidéoTraction™ system [47-51]. This method gives access to the true mechanical behaviour of polymers at a constant true strain rate. A geometrical defect is machined out in the middle of the gauge length of the dumb-bell shaped specimen to ensure the localization of the plastic deformation (necking). Seven ink markers are printed in this specific region, called Representative Volume Element (RVE). The axial true strain, ε_{33}, is obtained by a polynomial interpolation of partial strains measured from the displacement of axial markers using Lagrange Transform and following Hencky's

definition. For uniaxial tensile testing, the transversal strains in the RVE, ε_{11} and ε_{22}, are equal if the strain field is transversally isotropic in the center of the neck [52-56]. Lastly, the volume strain in the RVE, ε_v, is simply computed from the trace of the true strain tensor:

$$\varepsilon_v = \varepsilon_{11} + \varepsilon_{22} + \varepsilon_{33} \quad (3)$$

The volume strain can be positive, null or negative. In particular, when it is superior to zero it is called volume damage (since the "reversible" elastic part can be neglected), and in the opposite case (when it is negative) it is considered that a compaction mechanism is active.

The axial true stress, or Cauchy stress, is determined in the RVE, as the load per unit actual cross-section:

$$\sigma_{33} = (F/S_0) * e^{-2\varepsilon_{11}} \quad (4)$$

where S_0 is the initial cross-section at the RVE of the sample.

All the mechanical tests were performed at room temperature and at a constant true strain rate of 5.10^{-3} s^{-1}. This rate was chosen to ensure the control loop of the testing machine actuator, and it is slow enough to avoid self-heating of the sample [55, 56].

3.8. Scanning Electron Microscopy

Scanning electron microscopy (SEM) is used to observe the fracture surface of the different materials and then to enlighten the differences between the mechanical behaviours. To this end, *post mortem* micrographies are recorded using an environmental Quanta FEG 650 electron microscope from the FEI Company. The microscope parameters selected are a water vapor pressure of 100 Pa and an acceleration voltage of 4 kV.

4. Results and Discussion

4.1 Chemical analysis

Fig.2 a) shows the evolution of the gel content as a function of NH_2:MAH molar ratio between Jeffamine THF 100 and iPP-*g*-MAH polymers. Whatever the wt% of MAH, the gel content continuously increases with the amount of Jeffamine THF100 from 0, for the unmodified iPP-*g*-MAH polymers (0:1 molar ratio) to 12% and 46% for the CA 100 1:1 and G 3015 1:1 molar ratios, respectively. The null gel content values of the unmodified iPP-*g*-MAH polymers came from their low molecular weights induced by the MAH grafting reaction [1-11].

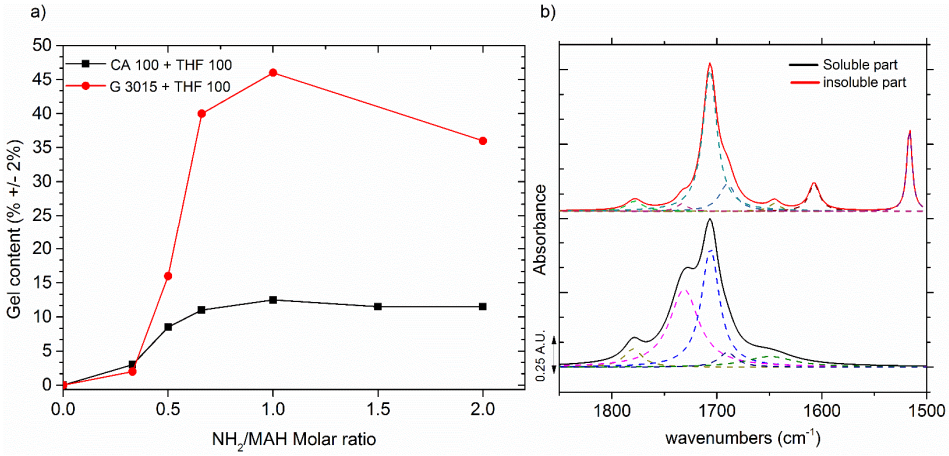

Fig.2. a) Gel Content evolution of CA 100 and G 3015 based materials after reaction with Jeffamine THF 100 at various molar ratio NH_2:MAH and b) FTIR spectra of the CA 100 1:1 soluble and insoluble parts.

The G 3015 1:1 gel content is three times higher than the one of CA 100 1:1. This difference could be explained by the difference of the grafted MAH weight fractions between both iPP-*g*-MAH, which vary from 1 to 3wt%. Between 0:1 and 1:1 molar ratios the gel content increases similarly for both materials. This could be explained by the crosslinking of the iPP-*g*-MAH chains that produces a 3D molecular network. For molar ratios higher than 1:1, an important difference between the two series of materials is observed. Whereas a plateau is reached for CA 100 at a gel content value of about 12%, there is a decrease from 46% to 36% gel content for G 3015 at a 2:1 molar ratio. The important excess of diamine in this last material (three times higher than in case of CA 100 for the same molar ratio) could be responsible for the decrease of the gel content value. As a matter of fact, when it is in excess, some molecules of diamine might only react with one MAH moiety, promoting thus a chain extension rather than a crosslinking. This was already observed with other diamines at high NH_2:MAH molar ratios [22-26].

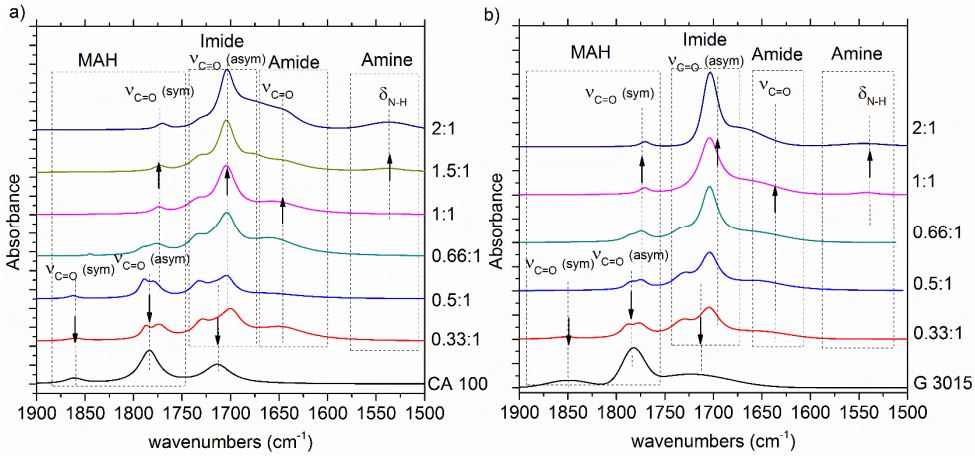

Fig.3. FTIR spectra of a) the CA 100 based materials and b) the G 3015 based materials as a function of the NH_2:MAH ratio.

In order to follow the evolution of the reaction as a function of molar ratio of the reactive species, FTIR analyses were performed and the spectra are presented in Fig.3. The spectroscopic vibrational band positions with respect to the chemical groups present in iPP-*g*-MAH polymers and in modified materials are given in Table S2 in SI. In the case of iPP-*g*-MAH polymer, the two characteristic vibrational bands at 1860 and 1780 cm^{-1} can be assigned to the symmetric and asymmetric $\nu_{C=O}$ vibrations of the

maleic anhydride group (MAH). The band at 1715 cm^{-1} could be assigned to $\nu_{C=O}$ vibrations associated to carboxylic groups formed by hydrolysis under wet storage conditions. By adding the Jeffamine THF 100, the intensity of the characteristic vibrational bands of the maleic anhydride group decreases to finally disappear when the 1:1 NH_2:MAH molar ratio is reached. In the meantime, one can observe the appearance of four new vibrational bands, among which the ones at 1770 and 1700 cm^{-1}, are assigned to the symmetric and asymmetric $\nu_{C=O}$ vibrations of the imide group, respectively. Indeed, upon the reaction of the diamine with the maleic anhydride two consequent addition-elimination reactions might take place to produce five-ring imides. The other two vibrational bands located at 1735 and 1650 cm^{-1} can be assigned to associated carboxylic acid/amide bonds, respectively. The amide bonds result from both reactions between carboxylic acid and Jeffamine THF100 and from the incomplete imidization reaction (opening of the anhydride ring without cyclization). The intensity of the band at 1700 cm^{-1} remained strong up to the 2:1 CA 100 material, but falls for the G 3015 2:1, with a raise of the imide bands, indicating a more complete reaction.

Finally, a broad bending vibration assigned to N-H bond can be observed at around 1550 cm^{-1} and could be due to the overlap of secondary amide and primary amino groups. The imide and amide/carboxylic acid bands describe the reaction between the primary amine brought by the THF 100 and the MAH groups grafted onto the polymers. The MAH bands evolutions indicate a complete consumption of the MAH groups by the reaction from the 1:1 equimolar molar ratio since they totally disappear. The absence of the primary amine band also confirmed the complete use of the amine groups for those materials. This evolution is in agreement with the gel content evolution from the 0:1 to the 1:1 sample for the CA 100 and the G 3015, which is maximum for the 1:1 molar ratio. In agreement with the gel content results, for this particular formulation, each MAH group reacts with one amino group, crosslinking thus iPP-*g*-MAH chains.

The presence of characteristic FTIR bands of the primary amine at molar ratios above 1:1 indicates indeed that the crosslinking agent is in excess or has not fully reacted. This might explain the stabilization for CA 100 based materials and the decrease of the gel content for the G 3015 based materials at molar ratios above stoichiometry. The peculiar decrease observed in case of G 3015 based materials is due to the excess of diamine, three times higher than in case of the CA 100 based materials. Some diamine molecules may only react with one MAH graft and that could be responsible for a chain extension instead of a crosslinking between the iPP-*g*-MAH macromolecular chains.

4.2. Microstructural characterization

It is well known that the crosslinking of a semi-crystalline polymer can change its microstructure because of the three-dimensional network, which may modify the macromolecular mobility and the chain segments length available for crystallization [17-22]. Those effects are thus investigated by performing one-dimensional WAXS and DSC experiments. The results are given in Fig.4, Fig.5 and numerically gathered in Table 2.

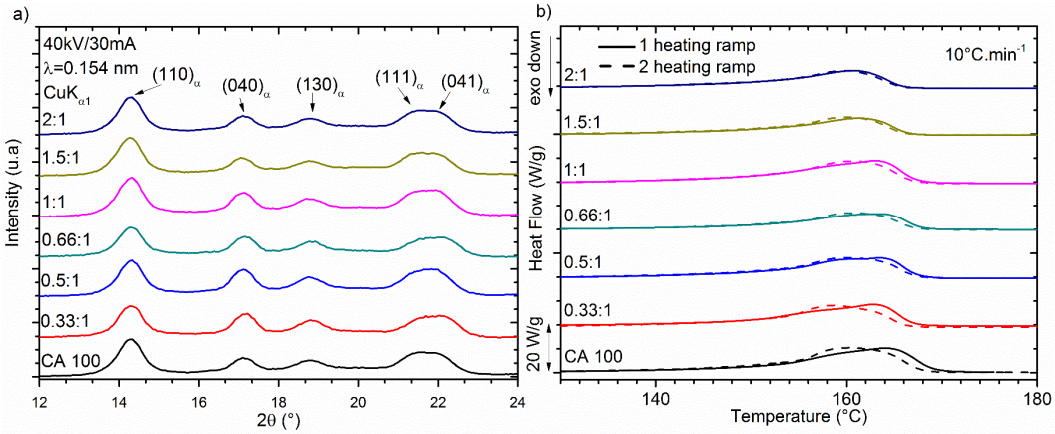

Fig.4. a) 1D WAXS diffractograms and b) DSC thermograms of CA 100 and its modified materials prepared at variable NH_2:MAH molar ratios.

The 1D WAXS diffractograms of CA 100 based materials (Fig.4 a)) exhibit characteristic peaks of a monoclinic α crystalline phase of iPP [44, 45]. The crosslinking reaction using THF 100 do not induce any modification of the crystallinity ratio, which remained of about 62%, as in the starting polymer. One can only observe some variations of the shape of the peaks and the values of the melting temperature range depending on the NH_2:MAH molar ratio and on the thermal history of the sample. In the case of the first heating endotherms, a decrease of the main melting temperature is observed with the increase of the NH_2:MAH molar ratio (from 165°C to 160°C between 0:1 and 2:1 molar ratios, respectively). On the second heating endotherms, small shoulders appear around 160°C up to a molar ratio NH_2:MAH of 1:1. Below NH_2:MAH equimolarity, this effect disappears probably due to the presence unreacted Jeffamine, in excess, which tends to facilitate the chains mobility. The decrease of the main melting temperatures and of the crystallinity ratios between the first and the second heating ramp would suggest an influence of the injection molding process on the semi-crystalline microstructures.

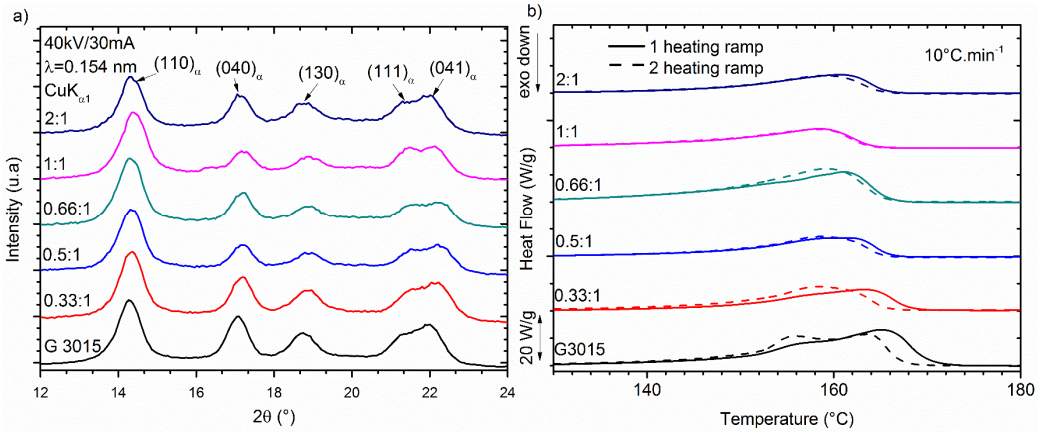

Fig.5. a) 1D WAXS diffractograms and b) DSC thermograms of G 3015 and the modified materials prepared at variable NH_2:MAH molar ratios.

Fig.5 shows the 1D WAXS diffractograms (Fig.5 a)) and the DSC thermograms (Fig.5 b)) of G 3015 based materials. Numerical values are reported in Table 2. Similarly to CA 100 based materials, the monoclinic α crystalline phase of the iPP can be identified on all WAXS spectra. However, a noteworthy difference can be distinguished since a decrease of the crystallinity ratio from 62% to 58% is observed and particularly for the highest NH_2:MAH molar ratio, of 2:1. Fig.5 b) shows the thermograms of the G 3015 based materials during the first heating revealing again the thermal history induced by

the injection molding process and a second heating resulting from a controlled cooling in the DSC apparatus at $10°C \cdot min^{-1}$. The melting temperatures ranges also confirm the presence of the monoclinic α crystalline phase of iPP. As previously observed with CA 100 based materials on their first heating thermograms, double shoulder shaped endotherms appear, but only until the ratio of 0.66:1. Again, in the case of the first heating, a decrease of the main melting temperature as a function of the increase of the NH_2:MAH ratio is also noticed from 165°C to 158°C for the ratios 0:1 and 1:1. Beyond that, the high quantity of THF 100 could be responsible for a unique crystalline lamellae thickness population. With large excess of diamine (ratio 2:1), T_m seems to increase beyond 160°C. The second heating thermograms show that the main melting temperatures are quite similar (close to 159°C) whatever the modified G 3015. Only a change of their melting temperature ranges is observable with a decrease of the minimum and maximum temperature values as a function of the increase of the NH_2:MAH molar ratio. G 3015 shows a double melting peak demonstrating its ability to generate two main crystallites size populations using a controlled cooling rate of $10°C \cdot min^{-1}$. Focusing on the crystallinity ratios determined from the first and the second heating ramp, it can be assumed that they are equal for a given NH_2:MAH molar ratio. Their trends to decrease are also similar as a function of the reaction degree, which is in good agreement with the previous WAXS result. The WAXS diffractograms and the DSC thermograms of the CA 100 and G 3015 based materials allow to characterize the impact of the new three-dimensional molecular network on the semi-crystalline microstructure of the different materials.

In the case of the matrices based on CA 100, the decrease of the melting temperatures implies, by using the Gibbs-Thomson relation equation (2), a decrease of the crystalline lamellae thicknesses, but without any modification of the crystallinity ratio. The three-dimensional molecular network presents here a direct influence on the crystallization ability of the materials. On the opposite, the G 3015 based materials which present a more complex three-dimensional network with a gel content three times higher than in case of CA 100's, shows a more significant impact of the crosslinking reaction. The obtained networks affect the melting temperatures and so the crystalline lamellae thicknesses of the polymers, but also the polymer chain mobility since a decrease of the crystallinity ratios is mentioned. To better describe the evolutions of the melting temperature ranges for the modified samples for both CA 100 and G 3015 based materials, SN/SSA studies were performed. The results of the SN protocol applied on the CA 100 polymer (polymer that exhibits the highest melting temperature of its series), are shown in supporting information. With those results, T_S temperatures were determined respectively at 169°C for the CA 100 and 167°C for the G 3015.

Fig.6 shows the last heating ramps of the SSA protocol for various CA 100 samples (Fig.6 a)) and the crystallite size distributions after deconvolution with the Fytik® software (Fig.6 b)). As expected, the unmodified CA 100 shows seven populations of crystalline lamellae thicknesses. Tightening of the crystallite size distribution towards smaller lamellae sizes is observed with the increase of the NH_2:MAH molar ratio. The thickest population of CA 100 (L_c = 19.8 nm) represents 2% of the overall crystallinity ratio. This population is provided from the crystallization of the longest polymer chain segments of the sample. The second thickest population (L_c = 15.5 nm) is the most important and represents 56% of the crystallinity ratio. The first population disappears from the 0.33:1 sample in favour to the second population proportion. This comment is also true, but in a lower intensity, for the 0.5:1 material. From the 0.66:1 molar ratio, it

is the second population that decreases in favour to the third one (L_c = 11.5 nm), which corresponds to even smaller chain elements. The crosslinking reaction, leading to a 3D network, disturbs thus the crystallization process of the longest chain elements. This leads to the disappearance of the thickest crystalline population followed by a decrease of the second one from the 0.66:1 NH_2:MAH molar ratio. This evolution of the crystallization ability of the longest chain elements explains the decrease of the melting temperatures range enlightened from the previous DSC results. The network building prevents the crystallization of the materials in favors of thinnest lamellae.

Table 2. Crystallinity ratio and melting temperatures of the different materials determined by DSC and WAXS analyses.

Materials		unmodified	0.33:1	0.5:1	0.66:1	1:1	1.5:1	2:1
CA 100	X_c (± 3%) (1st heating)	45	45	45	44	43	44	43
	T_m (± 1°C) (1st heating)	160/165	159/163	160/163	160/163	159/162	161	160
	X_c (± 3%) (2nd heating)	47	46	47	47	47	45	45
	T_m (± 1°C) (2nd heating)	161	159	160	161	160	161	159
	X_c (± 3%) (1D WAXS)	62	60	63	62	62	61	62
G 3015	X_c (± 3%) (1st heating)	50	48	47	47	44	--	42
	T_m (± 1°C) (1st heating)	157/165	159/163	159/162	157/161	158	--	160
	X_c (± 3%) (2nd heating)	50	48	47	47	46	--	42
	T_m (± 1°C)(2nd heating)	157/164	159	159	158	158	--	159
	X_c (± 3%)(1D WAXS)	62	62	61	61	60	--	58

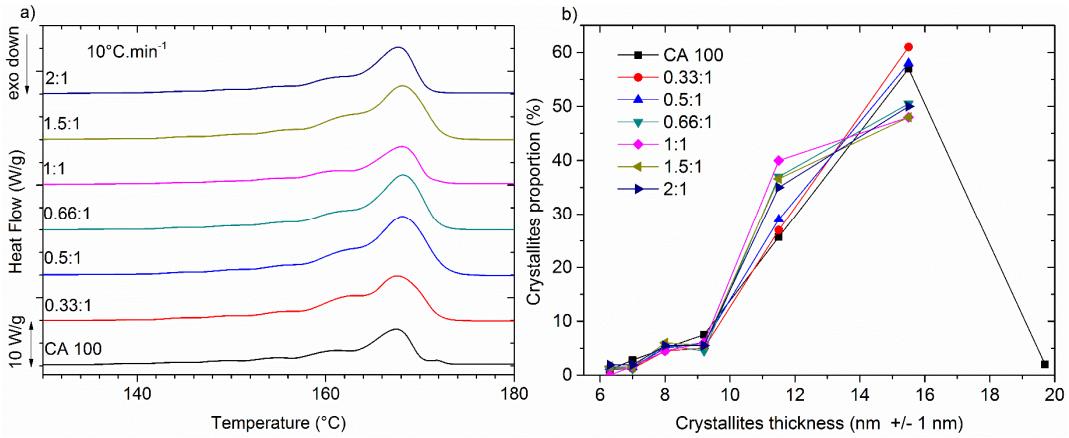

Fig.6. a) SSA last heating thermograms and b) distribution of the lamellae thickness populations according to T_s temperatures for CA 100 and its crosslinked materials.

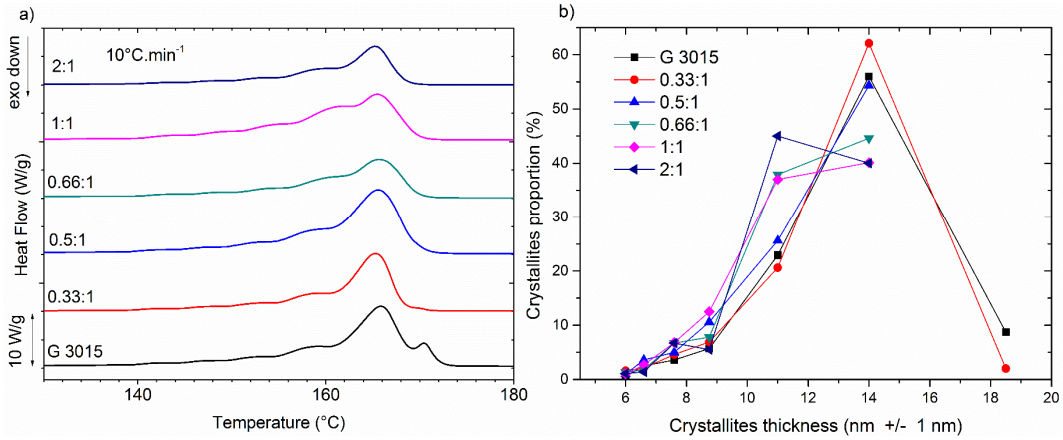

Fig.7. a) SSA last heating thermograms and b) distribution of the lamellae thickness populations according to Ts temperatures for G 3015 and its crosslinked materials.

Similarly to CA 100, G3015 shows seven sizes of crystalline populations (Fig.7). However, the thickest population (L_c = 18.5 nm) observed in the case of G 3015 and 0.33:1 material is 1 nm thinner than in case of CA 100. This difference could be explained by the higher MAH weight fraction and the smaller molecular weight of G 3015 [11, 29-34]. This population represents 9% of the overall crystallinity ratio for the G 3015 and only 2% for the 0.33:1 molar ratio and it disappears completely for the other materials. At the same time, the second thickest population (L_c = 14.5 nm) first raises from 56% for the unmodified G 3015 to 62% for the 0.33:1 sample and then decreases to 54% for the 0.5:1 and to 40% for the 1:1 samples. From the 0.66:1 to the 2:1, the third population (L_c = 11 nm), which corresponds to smaller chain segments, raises from 21% to 37% for the 1:1 material and finally to 45% for the 2:1. In the case of the CA 100 based materials, the second population remains the most important, but for the G 3015-based materials, the third population becomes equal in proportion to the second one. The three-dimensional networks of the G 3015 polymers are denser than the ones of materials based on CA 100. Then they exhibit a greater influence on the polymer crystallization ability, as discussed for DSC thermograms.

The three-dimensional network created by the chemical reaction shows here another difference between the two iPP-*g*-MAH. In the case of CA 100, the network affects the crystallization ability of the different samples, with a slight decrease of the melting temperatures range, as pointed out by SSA results. In the case of G 3015, with three times more MAH and gel content at equimolarity, the materials show a slight decrease of the melting temperatures range, but also a decrease of the crystallinity ratio. This second microstructure evolution is similar to that observed for other crosslinked polymers in the literature [17-22].

4.3. Mechanical properties

Fig.8 a) depicts the comparison of the DMA signals recorded for the storage Young modulus at a unique frequency of 1 Hz as a function of temperature for all the materials based on CA 100.

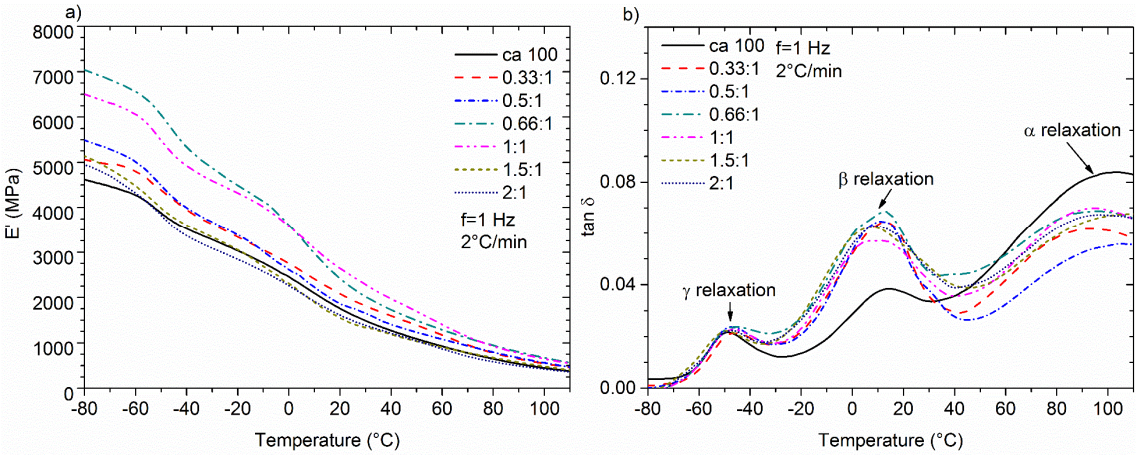

Fig.8. a) Evolutions of the storage Young modulus and b) the loss factor of CA 100 based materials.

The storage modulus values pointed out at low temperatures below 0°C tend to increase from the unmodified CA 100 to the 0.66:1 material. The increasing excess of diamine molecules may explain this phenomenon. Above 0°C, the elastic mechanical behaviour is stronger as long as the NH_2:MAH molar ratio increases until the equimolarity. This mechanical resistance improvement is clearly a consequence of the crosslinking reaction put in evidence by the FTIR analyses and the gel content results. When the crosslinking agent is introduced in excess, the elastic properties decrease progressively which means that THF 100 acts like a plasticizer. Fig.8 b) gives the evolutions of the loss factor at the same 1 Hz frequency as a function of temperature for all the materials based on CA 100. They all present the three relaxations already found for iPP [48]. The γ-relaxation associated with the motions of the methyl groups, has the same amplitude for all materials and occurs at around -40°C. The β-relaxation, associated with the glass transition of the iPP, stays close for the different materials at about 11°C, but presents different amplitudes. The crosslinking reaction during reactive extrusion, issued from the introduction of the THF 100 involves a change in the material architecture, which increases the amorphous phase contribution to the β-relaxation associated with the glass transition of iPP. Indeed, even without crystallinity ratio alteration, the amorphous phase disorder increases. This has resulted from an increase of the loss factor amplitude of the β-relaxation for the modified materials by the THF 100, compared with starting CA 100. The α-relaxation, associated to local motions within the crystalline phase, is located around 90°C for the various materials. The variations of amplitude of this relaxation could be explained by the weakest ability of modified matrices to crystallize in thickest lamellae in comparison to the unmodified CA 100.

In the case of the G 3015 materials it should be noted that due heterogeneities inside the molded plates, mechanical analyses could be performed only on materials obtained at molar ratios higher than 0.66:1 (Fig.9 a)). The 0.66:1 and 1:1 corresponding materials exhibit close Young modulus, and the same decrease for the 2:1 material is observed due to the same reasons as those discussed previously for materials based on CA 100. Fig.9 b) gives the evolutions of the loss factor for only the injectable materials based on G 3015.

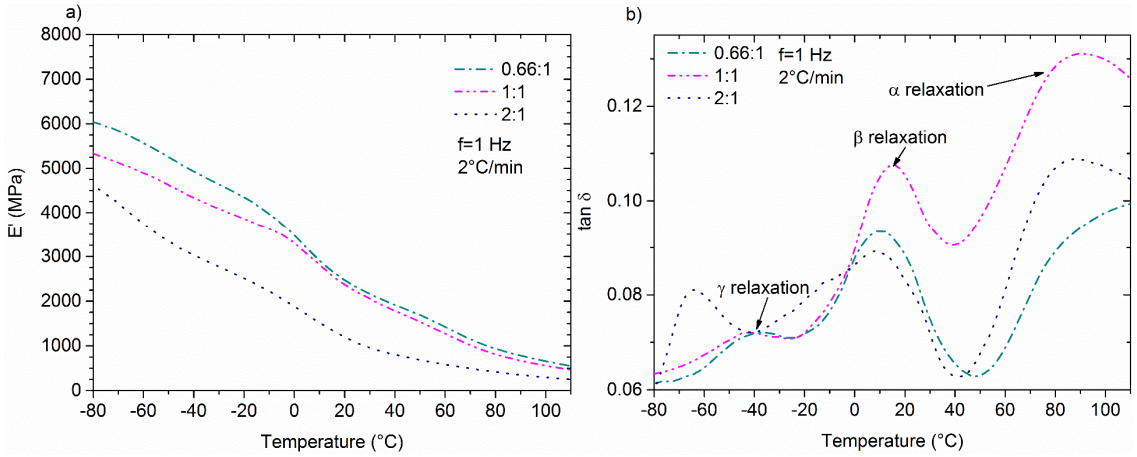

Fig.9. a) Evolutions of the storage Young modulus and b) the loss factor of G 3015 based materials

Materials G 3015 0.66:1 and 1:1, as materials based on the CA 100, present the three well-known relaxations found for iPP, while the material 2:1 presents several changes at low temperatures. The γ-relaxation associated with the motions of the methyl groups, has the same amplitude for materials 0.66:1 and 1:1 near -40°C. The temperature of the β-relaxation, associated with the glassy transition of the iPP, increases from 12 to 15 °C between the ratios 0.66:1 and 1:1, then decreases by 8°C for the material 2:1. The increase of the temperature associated with the glassy transition is logical in view of the crosslinking occurring which decreases the mobility of chains; this is highlighted by the chemical analysis of the materials. The decrease of temperature between the ratios 1:1 and 2:1 can be explained by the presence of molecules of diamine THF 100 in excess, which behaves as a plasticizing agent thus, they increase the mobility of chains and lower the temperature of the relaxation associated with the glassy transition. The more the material is crosslinked, the more the amplitude of the β-relaxation decreases being in agreement with a decrease of the mobility of chains. The α-relaxation, associated with local motions within the crystalline phase, is located close to 90°C for the various materials; however, the variations of amplitude of this relaxation are more difficult to explain. The material 2:1 presents important changes around the γ-relaxation and the β-relaxation at low temperatures compared to the two other materials. Besides the absence of the γ-relaxation typical of the iPP, a new relaxation between -65 and -60°C can be noticed, as well as a change of the shape of the β-relaxation at 8°C. This new relaxation can be associated with the glassy transition of the chains of poly (tetramethylene ether glycol)] / PPG (polypropylene glycol) copolymer composing THF 100 [35, 57-60]. Furthermore, the THF 100 in excess crystallizes at low temperatures. Its melting occurs at 8°C what could explain the appearance of a shoulder superimposed on the γ-relaxation of this material at low temperatures.

For further mechanical analysis at high true strain values, all the materials tested by DMA were studied with the VidéoTraction™ system in uniaxial tension deformation path. Fig.10 a) shows the true mechanical behaviours of the different CA 100 based materials. As expected, CA 100 presents a brittle mechanical behaviour with no plasticity due chains breaking induced by MAH grafting. The two materials with the lowest molar ratios (0.33:1 and 0.5:1) have also brittle mechanical behaviours similar to the one obtained for CA 100. The three-dimensional network in these cases is not sufficiently developed to improve the mechanical properties of the materials at high strains. The first significant change appears only from the 0.66:1 material which breaks

at a true strain value 15 times more important than in the case of the unmodified CA 100 ($\varepsilon_{b\ CA100}$ = 0.05 and $\varepsilon_{b\ 0.66:1}$ = 0.75). The molar ratio of this material is close to the one corresponding to the complete reaction, when NH_2 groups consume all MAH grafts. This next molar ratio 1:1 achieves thebest mechanical properties in terms of resilience and ductility. The true stress at break is more than twice higher than in the case of the unmodified CA 100 ($\sigma_{b\ CA100}$ = 33 MPa and $\sigma_{b\ 0.66:1}$ = 71 MPa). Moreover, the stress hardening is clearly stronger than in case of the previous molar ratio that could be explained by a higher level of molecular chains orientation towards the stretching direction. This result highlights that the optimum crosslinking degree that has been previously found regarding the gel content and the FTIR analyses and that does not induce important impact on the semi-crystalline microstructure (only a weak decrease of the crystalline lamellae thicknesses) is consistent with the material that presents the best mechanical properties. The two others materials, 1.5:1 and the 2:1, show also ductile behaviours, but with a significant decrease of the stress level compared to the 1:1 molar ratio material. Nevertheless, the amplitude of their stress hardening is not so much affected. This result can be explained by the excess of diamine molecules which acts here as a plasticizing agent as identified by the DMA results that promotes macromolecular chains mobility and then orientation.

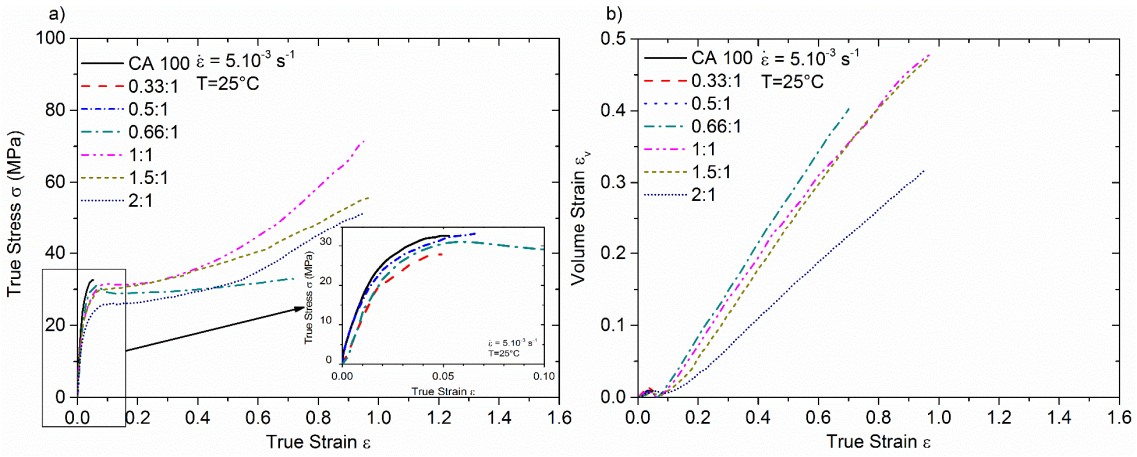

Fig.10. a) True mechanical behaviour laws and b) evolutions of the volume strain of the modified CA 100 based materials in uniaxial tension

Regarding the evolutions of volume strain as a function of true strain, uncompleted crosslinking encourages volume damage whereas diamine molecules excess decreases it, which is in good agreement with the shape of the stress hardening discussed in Fig.10 a).

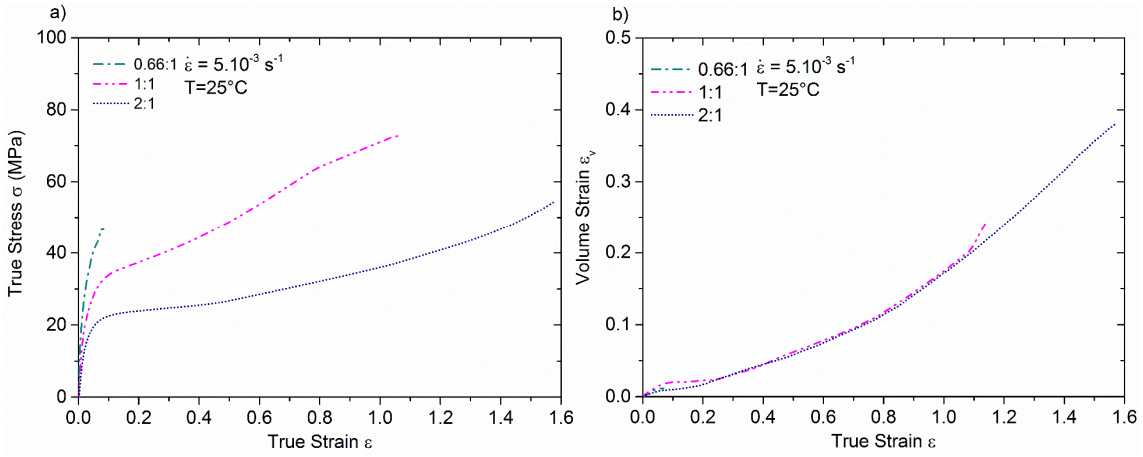

Fig.11. a) True mechanical behaviour laws and b) evolutions of the volume strain of the modified G 3015 based materials in uniaxial tensile tests.

Fig.11 a) shows the true mechanical behaviour of the G 3015 based materials. Like for the DMA analyses, only three materials were studied, the 0.66:1, 1:1 and 2:1 samples. In opposition with the CA 100 0.66:1 material, the G 3015 0.66:1 still present a brittle mechanical behaviour. The improvement of the mechanical properties occurs only from the 1:1 molar ratio. This material exhibits mechanical properties close to those of the CA100 1:1, with a ductile mechanical behaviour, and an important raise of true strain and true stress at break. The G 3015 2:1 samples also show a ductile mechanical behaviour, but with a raise of true strain at break, and a decrease of true stress level. Similar to the CA 100 2:1, this material presents the effect of the large excess of diamine molecules that act like a plasticizing agent. However, in this particular case of G 3015 2:1, the diamine molecules excess is three times higher than in case of CA 100 2:1 and so it induces in addition to a weaker stress resistance, the raise of true strain at break. This observed excess improves the deformation ability of the sample. These conclusions drawn from the true mechanical behaviours of modified G 3015 materials are corroborated by the evolutions of the volume strain depicted on Fig.11 b) since similar low volume damage is undergone during stretching.

To highlight such switch of true mechanical behaviour at large strains, SEM observations were performed on the fracture surface of the various samples. Micrographies are gathered in Fig.12. Fig.12 a) illustrates the unmodified CA 100 fracture surface and shows a classical brittle one in conformity with the determined true mechanical behaviour. The topography begins to change from the CA 100 0.66:1 material (image b)) with the development of a fibrillary microstructure on the most part of the sample surface. This morphology is complete with the CA 100 1:1 material (image c)) that exhibits the best true mechanical behaviour, with an important plastic deformation. It has to be noticed that fibrils were oriented along the stretching direction (perpendicular to the micrographies plane) and result from the creation of elongated voids. This evolution between the different CA 100 materials is in good agreement with the previous mechanical analysis. In case of the G 3015 materials, the d) micrography which corresponds to the fracture surface of the 0.66:1 material shows a brittle surface with some small regions where some fibrils can be observed. This indicates the beginning of the three-dimensional network influence on the mechanical properties. However, the network here is not sufficiently enhanced to induce the expected ductility. In case of G 3015 1:1 (image e)), a complete fibrillary microstructure is revealed, proof of the switch of true mechanical behaviour. A particular attention could be drawn on Fig.12 f) which shows an interesting zone of the

G 3015 2:1 fracture surface, it reveals the presence of some round elements on the fracture surface. They could be identified as THF 100 diamine molecules drops resulting of the large excess, which did not mix well with the polymer matrix. The same thing was not observed for the CA 100 2:1 material since the diamine excess is three times lower. Thus, these SEM observations confirmed really well the switch from brittle to ductile of the true mechanical behaviour from the 0.66:1 molar ratio in the case of CA 100 based materials and from the 1:1 molar ratio in the case of G 3015 based materials.

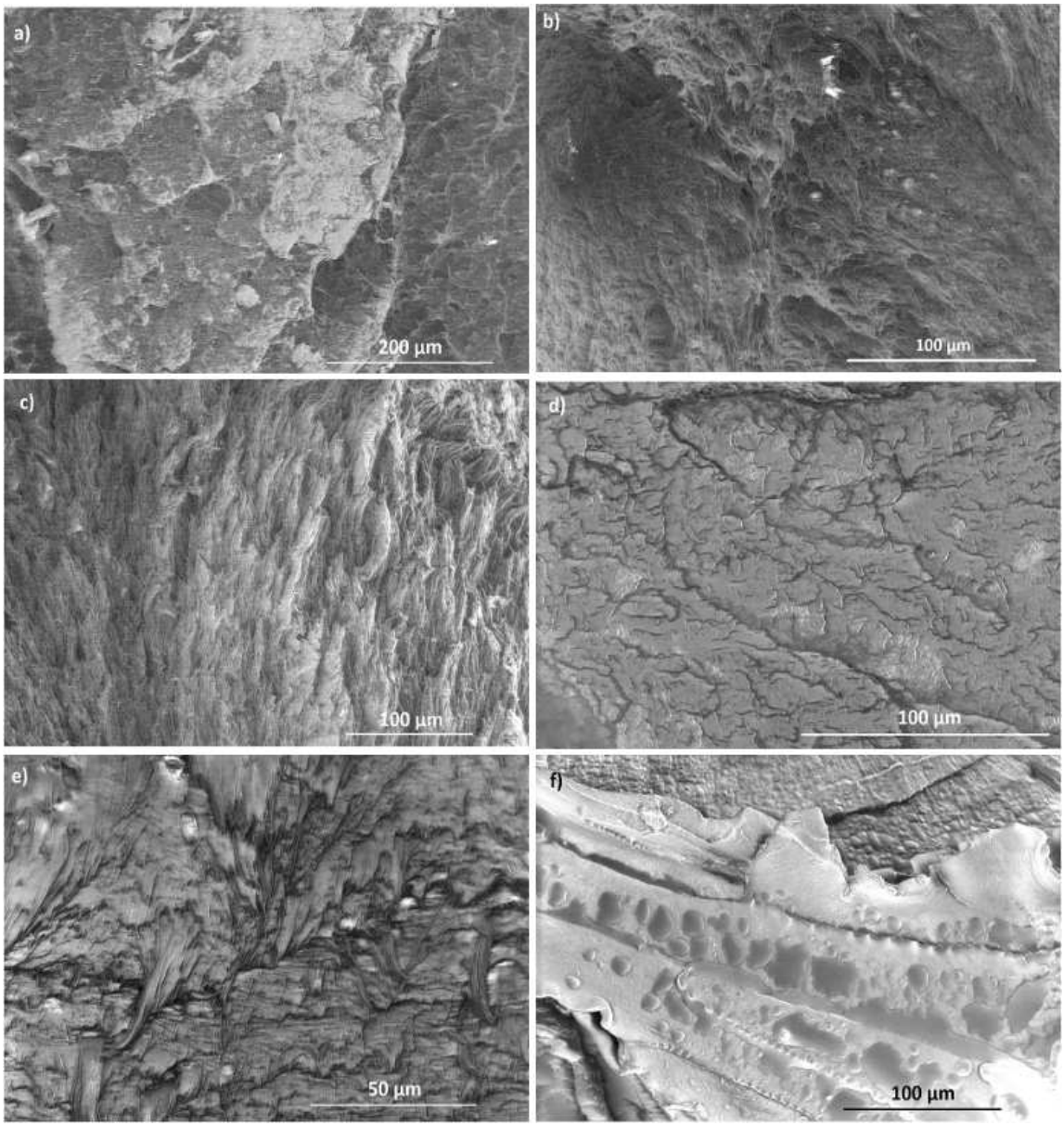

Fig.12. SEM observations of the fracture surfaces of a) unmodified CA 100, b) CA 100 0.66:1, c) CA 100 1:1, d) G 3015 0.66:1, e) G 3015 1:1, and f) and G 3015 2:1 materials.

Finally, to resume and to compare the real mechanical behaviours of all the materials of the study at large strain values (it means of the matter only without considering voids), intrinsic true mechanical laws were determined using the theory developed by Ponçot *et al.* in 2013 [51].

The remarkable shape of cavities in case of isotactic polypropylene is tube-like shape from the moment that volume strain intensity is high enough to have an influence on

the true mechanical parameters without significant change of shape. Thus, the intrinsic true strain in the axial direction can be expressed as follows:

$$\varepsilon_{33}^{i} = \varepsilon_{33} \qquad (5)$$

The expression of the intrinsic true stress may be given by:

$$\sigma_{33}^{i} = \frac{F}{S^{i}} = \sigma_{33}\frac{S}{S^{i}} = \sigma_{33}e^{\varepsilon_{v}} \qquad (6)$$

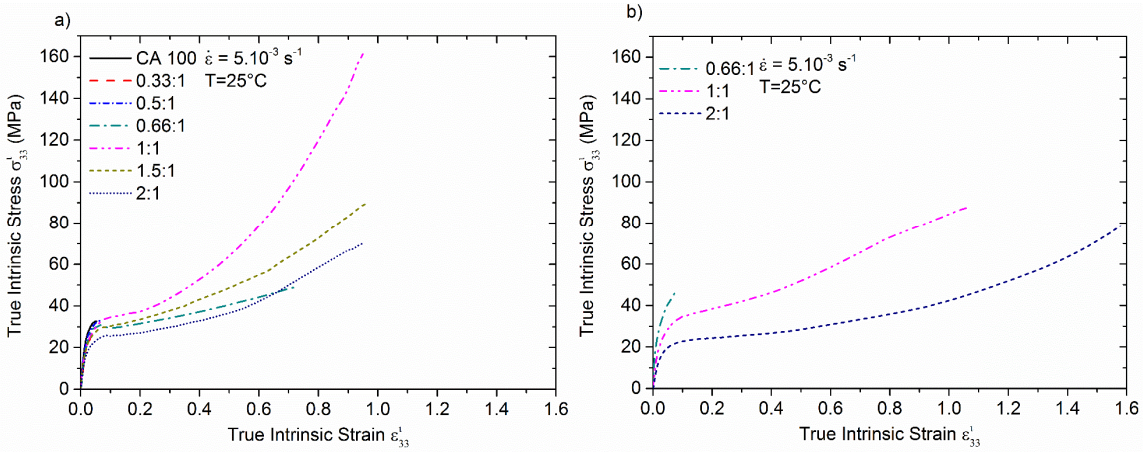

Fig.13. Comparison of the true intrinsic mechanical behaviours of a) the modified CA100 and b) the modified G 3015 based materials.

Fig.13 compares the intrinsic true mechanical behaviours of materials based on CA 100 (Fig.13 a)) to those of materials based on G 3015 (Fig.13 b)). By correcting the volume damage that occurs in such materials during uniaxial stretching, it can be observed that mechanical resistance increases as a function of the increase of crosslinking with a maximum for the 1:1 formulation for both iPP-*g*-MAH. The excess of diamine molecules decreases significantly the mechanical resistance due to its plasticizing effect. This phenomenon is extreme in case of the G 3015 2:1 material, but results to a large increase of the strain at break.

5. Conclusion

In-situ crosslinking of iPP-*g*-MAH bearing two weight fractions of anhydride (1 wt% for CA 100 and 3 wt% for G 3015) was performed through a twin-screw reactive extruder with a primary end-capping diamine, the polyether Jeffamine®THF-100. The crosslinking reaction had a direct impact on the microstructure of the polymer, resulting in a decrease of the crystalline lamellar thicknesses for both maleated iPP with an additional effect on G 3015, namely a slight decrease of the crystallinity ratio.

The most crosslinked networks and equivalent mechanical properties were reached at equimolar ratio of NH_2:MAH for which, interestingly, the gel content was three times lower for the CA 100 materials. In other words, one needs three times less Jeffamine to crosslink the 1 wt% iPP-*g*-MAH polymer to reach better mechanical properties such as resilience, yield and stress at break as with the richest MAH polymer. This could be due to the fact that the crystalline microstruture is poorer in the case of G 3015, while for both materials, the β-scission induced by the MAH grafting is counterbalanced by the formation of the 3D network.

More important, at a certain molar ratio (0.66:1 for CA 100 materials and 1:1 for G 3015 materials) the mechanical behaviour of the materials switched from brittle to ductile. When used in excess, the Jeffamine acts rather as a plasticiser, as the

crystallinity ratio and mechanical properties, such as Young modulus or stress level decreased.

Finally, it should be noted that the formulations presented herein are of particular interest for the design of composite materials, especially those that address structure-lightening topics. This is especially the case for CA 100-derived material functionalised at a 0.66:1 ratio and which exhibits a ductile behaviour while bearing reactive anhydride moieties available for further interact with other surfaces (i.e. carbon, metallic or metal oxides).

Acknowledgements

The authors thank the CINI Company for the extruder facilities and assistance in the process development, Huntsman, Eastman and Arkema for providing chemicals and polymers and Provisys Engineering Company for facilities with the VidéoTraction™ system. AL and MP thank the French Ministry for the PhD grant and the LabEX DAMAS for the financial support.

References

[1] Y. Minoura, M. Ueda, S. Mizunuma and M. Oba, J. Appl. Polym. Sci., 1969, 13, 1625–1640.
[2] R.M. Ho, A.C. Su, C.H. Wu and S.I. Chen, Polym., 1993, 34, 3264–3269.
[3] R. Zhang, Y. Zhu, J. Zhang, W. Jiang and J. Yin, J. Polym. Sci., Part A-1: Polym. Chem. 2005, 43, 5529–5534.
[4] S.H.P. Bettini and J.A.M. Agnelli, J. Appl. Polym. Sci., 2002, 85, 2706–2717.
[5] K. Cao, Z. Shen, Z. Yao, B. Qu, X. Pang, Z. Lu *et al*., Chem. Eng. Sci., 2010, 65, 1621–1626.
[6] R. Rengarajan, V.R. Parameswaran, M. Vicic, S. Lee and P.L. Rinaldi, Polym., 1990, 31, 1703–1706.
[7] V. Khunova and Z. Zamorsky, Polym. Plast. Technol. Eng., 1993, 32, 289–296.
[8] J.M. Garcia-Martinez, O. Laguna and E.P. Collar, J. Appl. Polym. Sci., 1998, 68, 483–495.
[9] F. Ide and A. Hasegawa, J. Appl. Polym. Sci., 1974, 18, 963–974.
[10] M.F. Diop, J.M. Torkelson, Polym., 2013, 54, 4143–4154.
[11] D. Shi, J. Yang, Z. Yao, Y. Wang, H. Huang, W. Jing *et al*., Polym., 2001, 42, 5549–5557.
[12] Y. Seo, J. Kim, K.U. Kim and Y.C. Kim, Polym., 2000, 41, 2639–2646.
[13] D.P. Harper, M.G. Laborie and M.P. Wolcott, J. Appl. Polym. Sci., 2009, 111, 753–758.
[14] J.Kubo, K. Otsuhata, S. Ikeda and T. Seguchi, J. Appl. Polym. Sci., 1997, 64, 311–319.
[15] Y.An, Z. Zhang, Y. Wang, J. Qiu and T. Tang, J. Appl. Polym. Sci., 2010, 116, 1739–1746.
[16] S. Bouhelal, M.E. Cagiao, D. Benachour and F.J. Baltá Calleja, J. Appl. Polym. Sci., 2007, 103, 2968–2976.
[17] S. Bouhelal, M.E. Cagiao, A. Bartolotta, G. Di Marco, L. Garrido, D. Benachour *et al*., J. Appl. Polym. Sci., 2010, 116, 394–403.
[18] S. Bouhelal, M.E. Cagiao, D. Benachour, B. Djellouli, L. Rong, B.S. Hsiao *et al*., J. Appl. Polym. Sci., 2010, 117, 3262–3270.
[19] S. Bouhelal, M.E. Cagiao, S. Khellaf, H. Tabet, B. Djellouli, D. Benachour *et al*., J. Appl. Polym. Sci., 2010, 115, 2654–2662.

[20] A.R. Padwa, Y. Sasaki, K.A. Wolske and C.W. Macosko, J. Polym. Sci., Part A-1: Polym. Chem., 1995, 33, 2165–2174.
[21] Z. Song and W.E. Baker, J. Polym. Sci., Part A-1: Polym. Chem., 1992, 30, 1589–1600.
[22] K.Y. Kim and S.C. Kim, Macromol. Symp., 2004, 214, 289–297.
[23] M. Köster and G.P. Hellmann, Macromol. Mater. Eng., 2001, 286, 769–773.
[24] B. Lu and T.C. Chung, Macromol., 1999, 32, 8678–8680.
[25] L. Cui and D.R. Paul, Polym., 2007, 48, 1632–1640.
[26] Q.W. Lu, C.W. Macosko and J. Horrion, J. Polym. Sci., Part A-1: Polym. Chem., 2005, 43, 4217–4232.
[27] A. Colbeaux, F. Fenouillot, J.F. Gerard, M. Taha and H. Wautier, Polym. Intern., 2005, 54, 692–697.
[28] F.P. Tseng, J.J. Lin, C.R. Tseng and F.C. Chang, Polym., 2001, 42, 713–725.
[29] Orevac® CA100, Technical specifications sheet by Arkema.
[30] R.M. Novais, J.A. Covas and M.C. Paiva, Compos. Part A, 2012, 43, 833–841.
[31] S. Butylina, M. Hyvärinen and T. Kärki, Polym. Degrad. Stab., 2012, 97, 337-345.
[32] Eastman™ G-3015 Polymer, Technical Data Sheet by Eastman.
[33] S.K. Nayak, S. Mohanty and S.K. Samal, Mater. Sci. Energy Eng. A, 2009, 523, 32–38.
[34] K.H. Wong, D.S. Mohammed, S.J. Pickering and R. Brooks, Compos. Sci. Technol., 2012, 72, 835–844
[35] Jeffamines® Polyetheramines, Technical specifications sheet by Hunstman.
[36] P.H. Hermans and A. Weidinger, J. Appl. Phys., 1948, 19, 491–506.
[37] Z. Bartczak, A. Galeski, A.S. Argon and R.E. Cohen, Polym., 1996, 37, 2113–2123.
[38] M. Kakudo and N. Kasai, X-ray diffraction by polymers, Kodansha Ltd, Tokyo, Japan, 1972.
[39] B. Wunderlich, Macromolecular Physics, Vol. 3: Crystal Melting, Academic Press, New York, 1980.
[40] D.C. Bassett and R.H. Olley, Polym., 1984, 25, 935–943.
[41] A.J. Müller, Z.H. Hernandez, M.L. Arnal and J.J. Sanchez, Polym. Bul., 1997, 39, 465–472.
[42] M.L. Arnal, V. Balsamo, G. Ronca, A. Sanchez, A.J. Müller, E. Canizales *et al*., J. Therm. Anal. Calorim., 2000, 59, 451–470.
[43] A.J. Müller, R.M. Michell, R.A. Pérez and A.T. Lorenzo, Eur. Polym. J., 2015, 65, 132–154.
[44] S. Ogier, C. Vidal, D. Chapron, P. Bourson, I. Royaud, M. Ponçot, *et al*., J. Polym. Sci., Part B: Polym. Phys., 2017, 55, 866–876.
[45] H. Chang, Y. Zhang, S. Ren, X. Dang, L. Zhang, *et al*., Polym. Chem., 2012, 3, 2909-2919,
[46] B. Fillon, J.C. Wittmann, B. Lotz and A. Thierry, J. Polym. Sci., Part B: Polym. Phys., 1993, 31, 1383–1393.
[47] C. G'Sell, J.M. Hiver, A. Dahoun, A. Souahi, and J. Mater. Sci., 1992, 27, 5031–5039.
[48] F. Addiego, A. Dahoun, C. G'Sell, and J.M. Hiver, Polym., 2006, 47, 4387–4399.
[49] C. G'Sell, J.M. Hiver and A. Dahoun, Int. J. Solids Struct., 2002, 39, 3857–3872.
[50] M. Ponçot, PhD Thesis, INPL-ENSMN, Nancy, France, 2009.
[51] M. Ponçot, F. Addiego and A. Dahoun, Int. J. Plast., 2013, 40, 126–139.
[52] C.B. Bucknall, D. Clayton, W. Keast, J. Mater. Sci., 1973, 8, p.514–524.
[53] S.I. Naqui, I.M. Robinson, J. Mater. Sci., 1993, 28, 1421–1429.

[54] B. Pukánszky, M. Vanes, F.H.J. Maurr, and G. Vörös, J. Mater. Sci., 1994, 29, 2350–2358.
[55] N. Billon, Mécanique & Industries, 2003, 4, 357–364.
[56] J. Ye, PhD Thesis, Lorraine University – LEMTA, Nancy, France, 2015.
[57] G. Wegner, T. Fuji, W. Meyer and G. Lieser, Die Angewandte Makromolekulare Chemie, 1978, 14, 295–316.
[58] L. Illinger, N.S. Schneider and F.E. Karasz, Polym. Eng. Sci., 1972, 12, 25–29.
[59] Q. Guo, R. Thomann, W. Gronski and T. Thurn-Albrecht, Macromol., 2002, 35, 3133–3144.
[60] R.A. Vaia, B.B. Sauer, O.K. Tse and E.P. Giannelis, J. Polym. Sci., Part B: Polym. Phys., 1997, 35, 59–67.

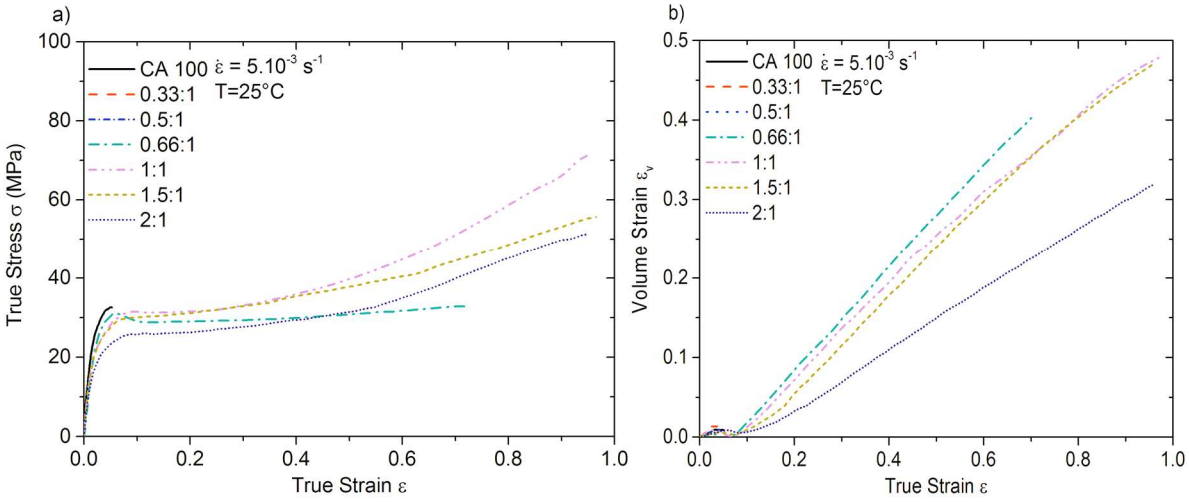

A slight crosslinking enables maleated isotactic polypropylenes to switch from brittle to ductile mechanical behavior with higher resilience than the most conventional one.